Enhanced Simulation of Coastal Compound Flooding through Fully-Coupled Modeling Framework

Ahad Hasan Tanim[1], F. Warren McKinnie[2], Erfan Goharian[1]

[1] *Civil and Environmental Engineering, University of South Carolina, Columbia, SC, 29208, USA*

[2] *Streamline Technologies, Winter Springs, FL 32708, USA*

Abstract

Coastal watersheds are vulnerable to compound flooding associated with intense rainfall, storm surge, and high tide. Coastal compound flooding (CCF) simulation, in particular for low-gradient coastal watersheds, requires a tight-coupling procedure to represent nonlinear and complex flood processes and interconnectivity among multidimensional hydraulics and hydrologic models. This calls for the development of a fully-coupled CCF modeling framework. Here, the modeling framework is centered around the development of interconnected meshes of the node-link-basin using the Interconnected Channel and Pond Routing (ICPR) model. The modeling framework has been built for a complex drainage network, consisting of tidal creeks, tidal channels, underground sewer networks, and detention ponds in Charleston Peninsula, SC. The floodplain dynamics of the urbanized peninsula are modeled by a high-resolution LiDAR-derived Digital Elevation Model (DEM) and Digital Surface Model (DSM), and overland flow is simulated by energy balance, momentum balance, or diffusive wave methods. The performance of the CCF model is tested for the 2015 SC major flood and 2021 tidal flood events. The momentum balance-based CCF model shows 98.35% efficiency in capturing street-level flooding location and the CCF model depicts that using the DSM potentially improves the simulation accuracy of the flood by 15-33% compared to LiDAR DEM. Moreover, it is found the momentum balance between surge arrival from a tidally influenced river and rainfall runoff plays an important role in flood dynamics in urbanized catchments. This study contributes to the existing knowledge of fine-scale floodplain dynamics in urban areas by enhancing the fully-coupled numerical representation of CCF processes.

Keywords: *Compound flooding; Fully coupled modeling; Flood Inundation Mapping; ICPR; DSM*

1. Introduction

The coastal compound flood (CCF) is a multi-driver (high river discharge, high tides, and intense rainfall) inundation process that happens in coastal areas (Bilskie and Hagen, 2018). Many coastal cities around the world (e.g., Cork (Ireland, 2009); Charleston (USA, 2015); Ravenna (Italy, 2015); Shoalhaven estuary (Australia, 2016)) are currently experiencing severe damages caused by CCF. A large number of these CCF events are caused by the combination of hurricane-induced intense precipitation, high sea level, high river discharge, and tides (Bevacqua et al. 2020). For instance, a highly populated area of Houston

suffered from a severe CCF incident in 2017, when Category 4 hurricane Harvey brought more than a meter of rainfall (~1,000-year return period) along with high storm surges from the ocean (Zhang *et al.*, 2018). The damage caused by the multi-variate flood drivers, simultaneously or in close succession, exceeds the probable impacts of the univariate flood drivers (Ikeuchi *et al.*, 2017). It is expected that more flood exposures and damages will be caused by CCF in the future, in particular in urban coastal areas with a more historical, cultural, ecosystem, and real-estate assets.

The magnitude of a CCF event is mainly governed by the nearshore surge characteristics, the coincident phase and amplitude of tides and the timing of the hurricane's landfall, the relative elevation of the coast with respect to sea level, and the rainfall intensity (Tanim and Goharian 2020a). On the other hand, climate change, by increasing the frequency and magnitude of heavy precipitation, river discharges, and sea level rise, intensifies the frequency of CCF events. For example, by the end of this century, the percentage of coastal areas experiencing CCF in Europe is expected to increase from 3% to 11% (Bevacqua *et al.*, 2019). This fact brought to scientists' attention the importance of considering the CCFs risk in flood resilience infrastructures. Recent studies have focused to provide a better perspective on compound flooding and estimating the probability of simultaneous occurrence of storm surges and intense rainfalls during the past few decades (Santiago-Collazo et al. 2019). However, there is a clear lack of multi-driver CCF inundation process-based modeling which undertakes a fully-coupled modeling framework.

An extensive review of previous studies shows that there has been only one study (Tang *et al.*, 2013) that truly used a tight-coupling procedure for CCF simulation (Santiago-Collazoet al. 2019). Other "arguably fully-coupled models" are in fact loose or one-way coupling techniques. A fully-coupled CCF model requires a complete representation and true spatial and temporal integration of the complex physical process and their mathematical equations devoted to fine-scale floodplain dynamics, and computational power, standards, and capacity required for modeling.

Fine-scale flood dynamics in densely urbanized regions, particularly the overland flow simulation, are mainly ruled by the drainage pattern, land use, and soil type. Fine-scale CCF modeling through an enhanced CCF model is vital for the simulation of the CCF factors' interactions and dynamic feedback between those, as well as for assessing the impact of flooding. Coarse-scale flood modeling underperforms in providing necessary flood hazard information for densely populated urban areas (Sanders *et al.*, 2020). Thus, fine-scale flood inundation maps (FIM) provide more informative flood hazard information for emergency managers and urban planners, which in turn prevents delays in emergency responses and evacuations, better access to care facilities and organizing emergency operations, and reduces disruptions and road closure (Navid *et al.*, 2022).

The modeling accuracy of CCF also depends on the integration/coupling tech-

niques used for linking hydrologic or hydrodynamic models and trading information between them. The CCF modeling can be performed using the hydrodynamic model or hydrologic model as a base model, which is linked to the other through a one-way coupling procedure (Tanim and Goharian 2020b). The one- and two-way coupling systems are defined by the exchange of information between 1D/2D overland flow module and the hydrologic model on specified time intervals for running models. Two-way coupling is often used for continental-scale hydrodynamic models (e.g., CaMa-Flood and GTSR, LISFLOOD-FP) to advance the understanding of CCF by taking into account the backwater effects from river discharge in coarse-scale CCF modeling (Ikeuchi *et al.*, 2017). Previous studies employed a 2D hydrodynamic model (e.g. Delft3D Flexible Mesh (Muñoz *et al.*, 2022) and SCHISM for creek-to-ocean scale 3D baroclinic model (Ye *et al.*, 2020)), coarse distributed hydrologic model (e.g. Gridded Surface/Subsurface Hydrologic Analysis (GSSHA) model (Karamouz *et al.*, 2017)), or 1D-2D coupled models (e.g. HEC-RAS 2D (Pasquier *et al.*, 2019); TUFLOW 2D (Shen *et al.*, 2019)) for CCF modeling. These models are either 1D-2D coupled or 2D coupled hydrodynamic models which refine complex land use configurations using flexible triangular mesh or rectangular grids using energy or momentum-based continuity equations. However, in order to achieve a fully coupled model, all of the physical processes' governing equations should be solved at the same time (Santiago-Collazo et al. 2019). Still, a real fully coupled model for CCF simulation for a complex coastal setup is missing to represent the uncertainty associated with the models' boundary conditions.

CCF includes non-linearity in its physical processes. Prior studies have engaged 1D/2D flood models and statistical methods therewithal to estimate the uncertainty and interdependency of the boundary conditions of CCF among the flood hazard drivers e.g., storm surges and extreme rainfall. The CCF events have significant interdependence on rainfall extremes and storm surges in coastal cities (Wahl et al. 2015). The hydrodynamic models cannot accurately simulate CCF systems because hydrodynamic models assume that channel or overland flow routing is only a function of boundary conditions, roughness factors, and terrain elevation; thus, the importance of rainfall-runoff effect has been ignored (Saksena *et al.*, 2020). Moreover, the river reaches or links do not interact with the subsurface flow, which can play a dominant role in the momentum balance during a CCF. Simulating floods using a hydrodynamic model requires both upstream and downstream flood boundary conditions to be updated continuously and it is very sensitive to the lateral flows generated by adjacent surface and vertical fluxes from precipitation and evapotranspiration. Even incorporating the rain-on-grid options with 2D hydrodynamic models, such as LISFLOOD-FP, HEC-RAS 2D, and FLO-2D, have limited applications in CCF due to their inability to integrate the hydrologic flux and processes which account for all physical process of CCF. The hydrodynamic models for CCF simulation, on their own, cannot provide realistic estimates of fluxes at boundaries (Jafarzadegan *et al.*, 2021). Thus, a fully coupled modeling system is required to represent a rain-on-grid alternative that is capable of capturing the non-linearity of CCF

physics (Jafarzadegan *et al.*, 2021). A successful example of a tightly coupled CCF model, offered by Tang et al. (2013), deployed a hydrologic model and linked it into an existing loosely-coupled hydraulic/ocean circulation model for the New Jersey (US) coastline (i.e. FVCOM and Shallow Water Model). However, this model still has several limitations, which is later addressed in this study, in particular for hydrologic modeling, as it does not consider any infiltration, precipitation losses, or routing mechanism (Santiago-Collazo et al. 2019).

Table 1 shows newly developed models and offered modeling frameworks since the comprehensive review of compound inundation models conducted in 2019 by Santiago-Collazo et al. (2019). Another alternative for coupling, still one-way or loose coupling, is when a hydrologic model has been mainly used for CCF simulation and a hydrodynamic or ocean circulation model is linked to it (Table 1). However, this one- or two-way coupling system is not adequate to represent the nonlinearity of the CCF overland flow process. Lumped hydrologic models are also inadequate in capturing the runoff process of highly urbanized coastal watersheds because the land cover features are complex and the runoff process has significant influence from complex land use systems. Results from the hydrologic model would be oversimplified by assuming homogenous soil profiles, and land cover types throughout a watershed (Kuchment and Gelfan, 2002; Leander and Buishand, 2007; Paquet *et al.*, 2013).

The nonlinearity involved in momentum, energy, and mass balance in CCF results in improper FIM, which is mostly the case for conventional hydrodynamics models, because of the neglect of the acceleration components for flood routing processes in overland flow generation. The tidal flood propagation in 1D hydrologic models routing process (SWMM, HEC-HMS) for CCF modeling allows water to exit just at drainage/channel outlets and neglects the coastline boundary as a whole. This potential limitation underestimates the magnitude of CCF and inundations in 1D model because tidal floods can propagate through tidal wetlands, or coastal areas having lower elevations below sea level at any place on the coastline.

All in all, the majority of CCF modeling framework suffers from one or several issues, including *i)* overdependence on simplified modeling techniques such as coarse-resolution model domain representation, *ii)* overlooking the nonlinearity of overland flow process, land use-runoff interaction with engaging loose coupling technique in hydrologic-hydraulic models, and *iii)* lack of innovative solutions for incorporating the tidal regimes from the ocean-river interface in the model domain (Saksena *et al.*, 2020). To address these issues, the CCF's overland flow modeling should represent fine-scale flood dynamics in an urbanized area with complex land use types to fully couple distributed hydrologic and 2D hydrodynamics models for enhanced CCF modeling and FIM. However, precise topographic information and land use maps are required to develop such distributed hydrologic models with fine-resolution hydrologic units to capture the complete physics of CCFs.

Table 1: Literature reviews on the CCF model and their coupling scheme

Literature	Model	Couplin
Muñoz et al. (2021)	Deep learning	Multi-sou
Jang and Chang (2022)	Hydrodynamic and Copula model	Hydraulic
Shi et al. (2022)	SWMM and ADCIRC, a two-dimensional (2D) hydrodynamic model	Tight cou
Joyce et al. (2018)	ADCIRC and ICPR	One way
Kupfer et al. (2022)	Delft3D	Wave and
Čepienė et al. (2022)	HEC-RAS	
Jafarzadegan et al. (2021)	HEC-RAS2D and LISFLOOD FP	

Distributed hydrologic models should represent spatial variations of model parameters and distributed catchment hydrologic processes by incorporating variations in topography, land use, land cover, soil class, and precipitation data which can enhance the FIM of CCF. The spatial configuration of land use, in particular, has a prominent impact on flood peak, peak discharge, and runoff volume. The NRCS curve number (CN) model is a widely accepted approach for urban rainfall-runoff simulation. In highly urbanized areas, the curve numbers act as a representative index of runoff potential from rainfall, based on different land classes (Walega *et al.*, 2020). The CN method estimates surface runoff based on a catchment's physical properties, antecedent soil moisture conditions, and antecedent rainfall 5-days before the storm (Mishra et al. 2013). In lumped hydrologic models, the discretization of curve numbers is done by weighted area curve number estimation, which leads to inaccurate rainfall-runoff estimation. Distributed hydrologic systems should be discretized based on fine-scale hydrologic units, which contain unique hydrologic model parameters, such as land use and soil type, at a fine scale. To represent the topography of hydrologic units, data from modern LiDAR systems is precious. Such data must be fused with digital map data, building topology, and land use to maximize the information contained therein (Hunter *et al.*, 2008).

Due to more frequent storms, high tides, and sea level rise, highly urbanized peninsulas or low-gradient coastal areas connected by tidal creeks are more susceptible to CCF and are at the frontline of sea level rise impacts. In order to provide a better understanding of multi-hazard-driven flood processes, the multidimensional physics and nonlinear interactions between hazard drivers should be considered in an integrated manner and fine scale. Consequently, in order to address the modeling framework limitations and resolve deficiencies to improve compound coastal flooding simulation for urbanized regions, the overarching objective of this study is to develop a fully-coupled model which represents the underlying non-linearity and multi-dimensional integration of CCF. To achieve this objective, the fully-coupled modeling system should encompass features that are described below:

1. A true fully-coupling procedure to integrate a hydrodynamics model with a distributed hydrologic model in a single modeling platform by synchronized run time marching.

2. An enhanced representation of CCF multi-dimensional physics, by adopting appropriate dimensions for hydrologic and hydrodynamic systems through a selection of more sensitive dimension(s) of the systems for CCF, such as one-dimensional underground drainage networks, and detention ponds, two-dimensional tidal creeks and wetlands, 2D overland flow processes and distributed hydrologic modeling.

3. A fine-scale distributed modeling system that improves the urban flood dynamics by a representation of complex land use-runoff interactions and GIS-based data assimilation.

The current study deploys the Interconnected Channel and Pond Routing (ICPR; Saksena, et al. 2021; 2019; Saksena et al. 2020) model to develop a fully-coupled model of CCF for the Charleston Peninsula in South Carolina. Charleston peninsula's complex land setting and strategic location make it an ideal test bed for CCF modeling. The CCF model outcome is validated using South Carolina Department of Transportation (SCDOT) road closure reports and USGS high water marks data.

1. Methodology

2.1 Model description

In the current study, a fully-coupled modeling system is developed through fine-scale integration of parcel-level hydrology by utilizing flexible) triple meshes (triangular irregular network (TIN), honeycomb, and diamond) to answer unexplored questions of CCF modeling regarding the non-linearity of multi-hazard drivers and multi-dimensional physics. The ICPR model deploys a spatially flexible TIN mesh network (using the finite volume method to discretize the model's domain) to capture the physical characteristics of the watershed, floodplain, and drainage networks. The model's three building blocks (node, link, and basin) applying triple mesh intercommunication create the opportunity for integrated modeling of CCF. ICPR links 2D overland flow and surface hydraulics equations with a set of underlying hydrologic and pipe hydraulic equations and solves these equations simultaneously on each time step. This allows for the basin rainfall-runoff information to be exchanged with links (e.g. subsurface storm sewer system, detention ponds, tidal channels, and tidal creeks) in a fully integrated system.

The basins in ICPR are represented by honeycomb meshes (Fig. 1). The honeycomb mesh acts as a control volume which is constructed by joining the midpoints of the triangle sides of the TIN, which then represents a hydrologic unit (Fig. 1). The mass balance equations are solved for each honeycomb and surface runoff is calculated for each basin (ICPR, 2021a). Then the runoff information is passed to the nodes of triangular mesh (Fig. 1) after a certain coupling interval using a time marching scheme called FIREBALL (ICPR, 2021a). The FIREBALL method uses a numerical technique based on the second-order Runge Kutta method (ICPR, 2021b). The time marching scheme transfers and updates the boundary conditions from surface hydrology blocks to hydraulics

blocks. The coupling process provides spatiotemporally adaptive hydraulic time stepping for simulating the fully distributed hydraulics-hydrology (Saksena, et al., 2019, 2021; Saksena et al., 2020).

The ICPR model determines the incremental changes of the stage at each node based on the continuity equation (Eq. 1). Then, in Eq. (3), the node inflow is calculated by summing up $Q_{\text{link}_{\text{in}}}$(sum of all flow incoming to a control volume), Q_{excess} (direct runoff due to rainfall excess) and Q_s, where the later is the seepage flow contribution from the groundwater model.

$$dz = \left(\frac{Q_{\text{in}} - Q_{\text{out}}}{A_{\text{surface}}}\right) \text{dt} \tag{1}$$

$$Z_{t+dt} = Z_t + \text{dz} \tag{2}$$

$$Q_{\text{in}} = \sum Q_{\text{link}_{\text{in}}} + \sum Q_{\text{excess}} + \sum Q_{\text{external}} + \sum Q_s \tag{3}$$

$$Q_{\text{out}} = \sum Q_{\text{link}_{\text{out}}}$$

where dz denotes the incremental change in stage and Q_{in} and Q_{out} are the total inflow and outflow rates to and from a node, respectively. A_{surface} is the wet surface area which is calculated for each node, and the computational time step is defined by *dt*. $Q_{\text{link}_{\text{in}}}$ and $Q_{\text{link}_{\text{out}}}$ are the sum of all incoming discharge and outgoing discharges from the control volume or honeycomb mesh respectively. Z_{t+dt} is the water surface elevation (WSE) at time step $t+dt$ which can be obtained from Eq. (2) using Z_t (WSE from the previous time step). The direct runoff from a control volume is calculated using the NRCS curve number method.

The honeycomb meshes represent the catchment areas that are used for the subsurface processes' integration with surface hydrology too. Each honeycomb mesh in ICPR is intersected with multiple map layers (i.e., soils, land cover, rainfall) and discretized into sub-polygons, where each unique combination is used for the estimation of rainfall-runoff (Fig. 1d). Infiltration is estimated for each sub-polygon based on its imperviousness and other characteristics (Fig. 1d). Rainfall excess from each of the sub-polygons is aggregated in honeycombs, and then they are assigned to their corresponding nodes in the triangular mesh (Fig. 1a), also known as 2D nodes in ICPR.

In a drainage system, a "node" is used to receive the energy, mass, or momentum continuity (inflow and outflow) characteristics to calculate the Water Surface Elevation (WSE) for a particular location (Saksena et al. 2020). The "links" are used to convey the WSE information from one node to another. The discharge at any link is calculated based on the physical properties and control specifications of upstream and downstream nodes. To minimize the computational steps, the node linkages are represented by a flexible TIN which can be refined or coarsened at the desired resolution following rules of mass balance. The vertices of each TIN are treated as the center of a control volume or honeycomb mesh (Fig. 1). Once rainfall excess occurs, it is directly/instantaneously applied

to the associated 2D node of the related honeycomb. The surface water then flows through the system and along the triangular sides of the TIN and the 1D hydraulics elements such as pipes. When the nodes in TIN have reached the overflow conditions and the drainage system reached the drainage capacity, overland flow occurs and diamond mesh comes into action (Fig. 1c).

This study further enhances the CCF modeling in ICPR by introducing a parameter called edge length factor (ELF) for model sensitivity analysis for optimizing the flood depth and duration. For this purpose, we have used the coupling scheme proposed by Saksena et al. (2020; 2019; 2021) for the ICPR model. Water flows along the triangle edges are estimated based on an equivalent rectangular geometry approximation. Eq. 4 is used to calculate the average length and width of equivalent rectangular geometry.

$$W = \frac{A_{\text{Diamond}}}{f * L} \tag{4}$$

where, f and W are the edge length factor (ELF) and the average width of an equivalent rectangle, respectively. L is the distance between two adjacent vertices of a triangle in a TIN. A_{Diamond} is the area of the diamond mesh polygon. While it is not possible to exactly account for all the storage and intricate flow paths in a system with 2D models, the calibration of ELF provides a mechanism to mitigate these errors. For example, as soon as the ELF increases, the width of the rectangular channel reduces, which in turn causes delaying the water flow through the triangle mesh edges and effectively attenuates the flow.

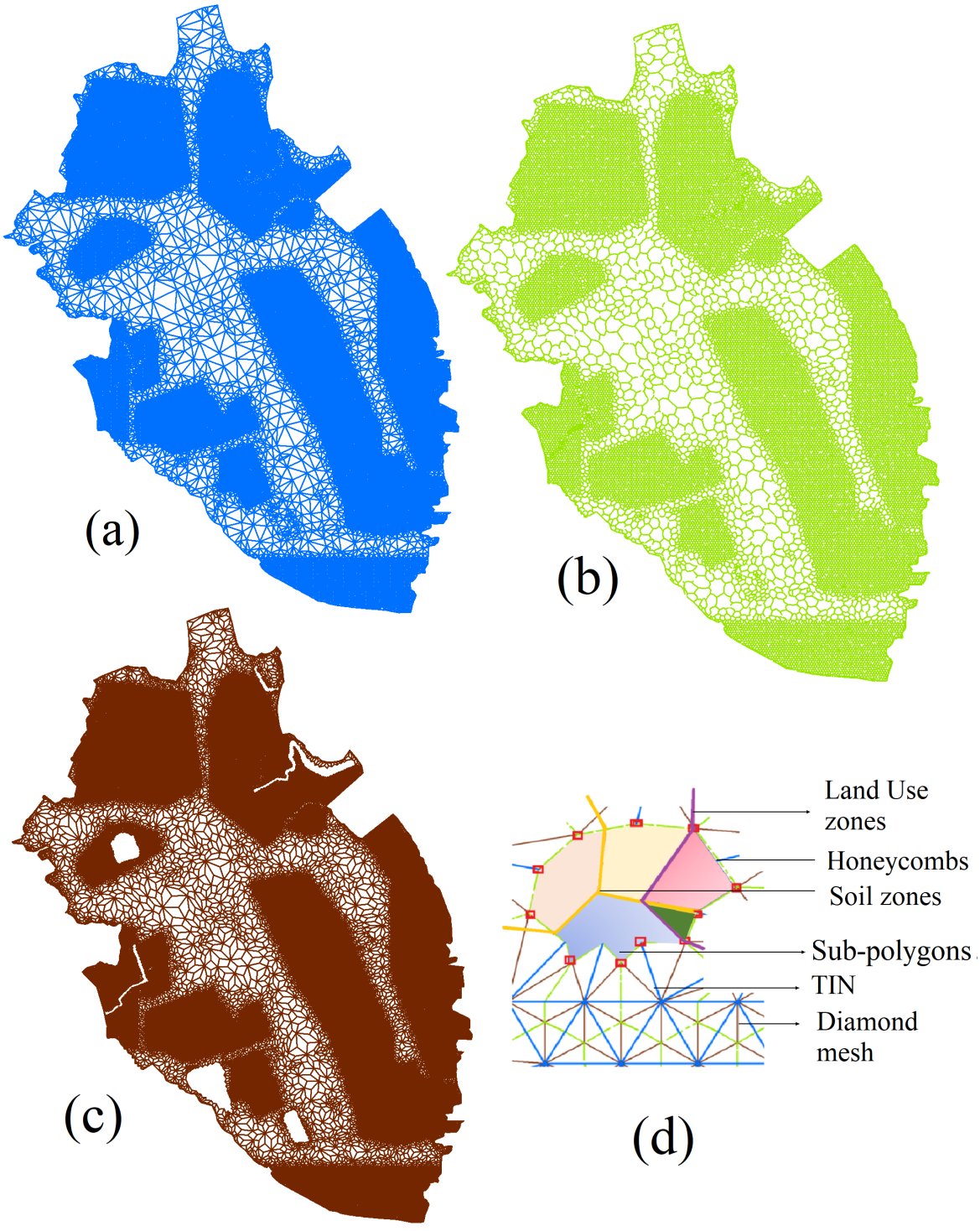

Fig. 1 The adopted (a) TIN mesh for terrain characterization, (b) honeycomb mesh for basin characterization

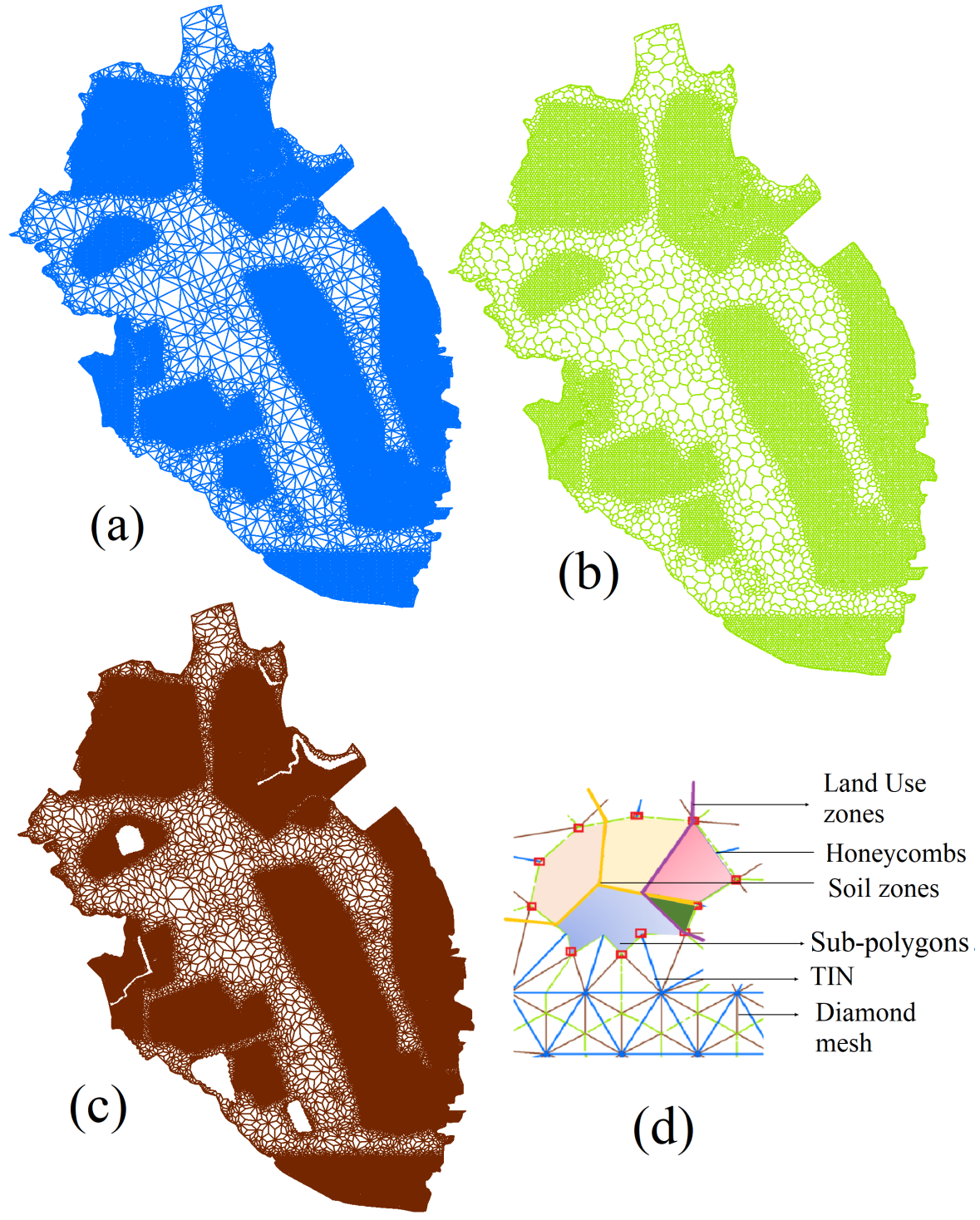
(a)
(b)
(c)
(d)
Land Use zones
Honeycombs
Soil zones
Sub-polygons
TIN
Diamond mesh

The TIN mesh is also used to develop a diamond mesh layer around the triangle sides (Fig. 1c). The diamond meshes are extended from the honeycomb centroids and are reformed into equivalent rectangles with an average 2D slope. For 2D overland flow modeling, ICPR employs the diamond mesh layer (Fig. 1c) where the physical characteristics of the floodplain are represented by the roughness based on the land use types. ICPR computes the 2D overland flow using momentum, energy, or diffusive wave equations. These equations are lumped at TIN mesh edges to support surface water propagation in 2D space. The diamond meshes are mainly intersected with the land uses, such as developed land use, that require the damping threshold and area reduction factor for the 2D overland flow region. The energy damping threshold is applied for the overland flow propagation over the developed land use, particularly the building rooftops. The area reduction factor can compensate for the obstructions of trees and landscapes over the floodplain (ICPR 2021a). With 2D links, such as open channels, the runoff is routed over the surface for the drainage area within the floodplain or overland flow region. ICPR model allows spatially varying roughness coefficients which depend on land use types and depth varying (deep and shallow) roughness. An exponential decay function is used for calculating the depth-varying roughness coefficient (Saksena et al., 2019). This is one of the main advantages of ICPR over other hydrodynamic models such as HEC-RAS 2D, Delft3D, and LISFLOOD -FP to simulate the CCF in the coastal urban area.

The fully-coupled modeling framework is shown in Fig. 2. Three main modeling components of the system: 1) Channel and Pond routing, 2) Overland flow region and 3) Distributed hydrologic system along with their interconnections and spatiotemporal inputs are shown in this flowchart (Fig. 2). In the following sections, first the study area is presented (Section 2.2), then required model inputs and pre-processing of data, including GIS data assimilation, are discussed in detail (Sections 2.3). Section 3 describes the model setup process, model parameterization, and sensitivity analysis.

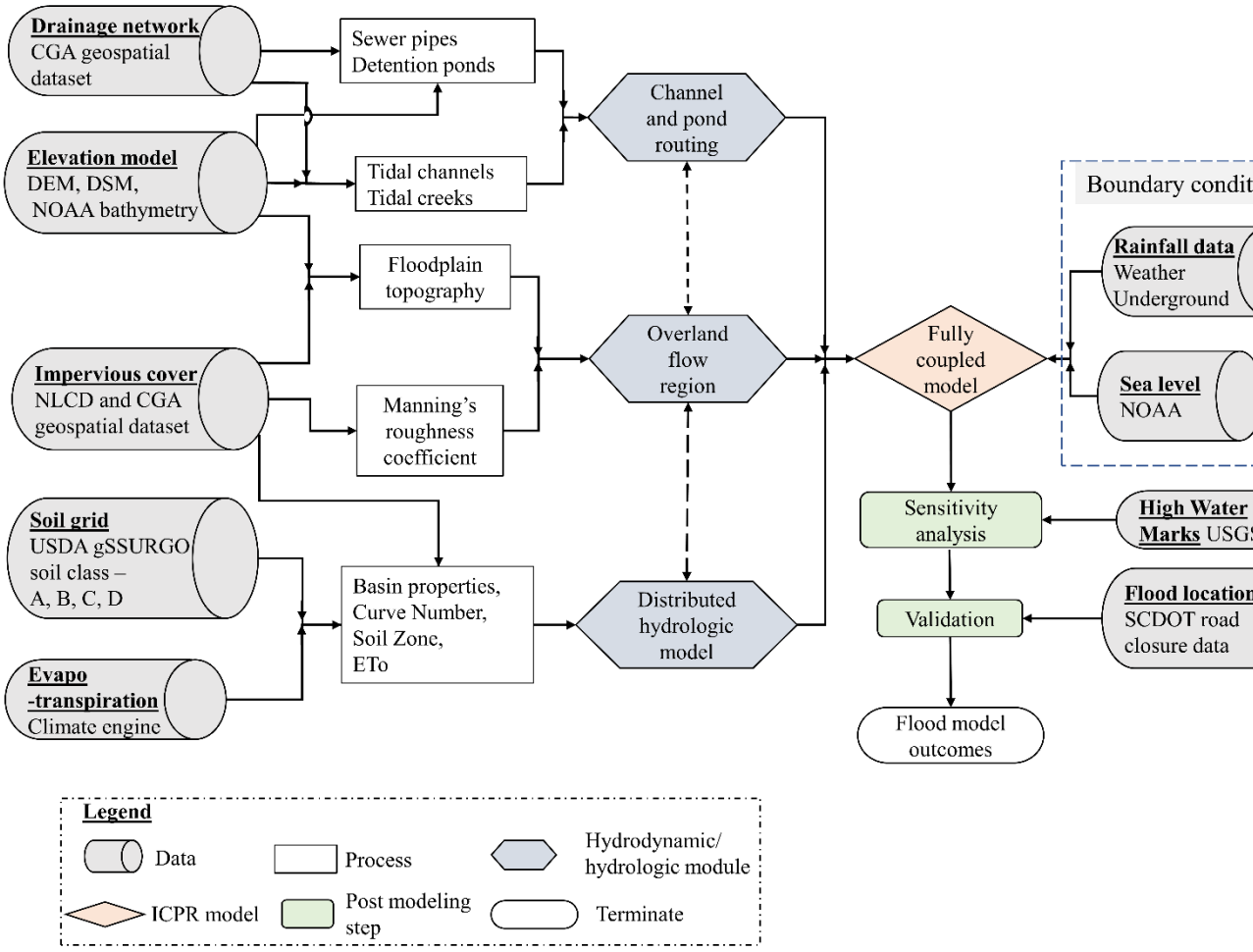

Fig. 2: The CCF modeling process diagram in ICPR

2.2 Study area

The fully-coupled CCF modeling in this study focuses on the compound flooding problem of the Charleston peninsula, SC, USA. Charleston peninsula is an economic powerhouse for tourism, trade, and industries in SC, but now it is impacted adversely by more frequent incidents of flooding and hurricanes. The Charleston harbor and port are regarded as one of the southeastern United States' fastest expanding container ports. The port's contribution in terms of economic value is ranked eighth in the United States, generating around $26 billion in trade revenue each year (Morris and Renken, 2020). Due to the low elevations of the drainage system and tidal interconnections to the adjacent Ashley and Cooper Rivers (Fig. 2), flooding from hurricanes, tropical storms, tropical depressions, and high tides threatens a large portion of the peninsula

(USACE, 2020). The potential damage of CCF highly depends on the timing of a coastal storm and the rainfall intensity. The peninsula's aerial extent is rather small, and numerous tidal creeks can accelerate tidal surge propagation. During high tides, the landfall of storm surges near Charleston may lead to a disastrous event and high risk to the city as the peninsula is located at the estuary (Fig. 2). Hurricane Hugo (1989) is the worst recorded hurricane that has affected Charleston peninsula. The hurricane caused a damage cost of about $10 billion and caused 27 deaths throughout the Carolina coasts (NRC, 1994). The SC flood of 2015 is another notable flood the Charleston peninsula has experienced.

The complex urban drainage system of Charleston consists of underground sewer pipes, tidal creeks and channels, woody wetlands, emergent herbaceous wetlands, and detention ponds (Figure 3). The drainage outlets are tidally influenced by the surrounding sea and tidal rivers. The detention ponds allow for surface water storage during floods. The underground drainage system is a key element to collect and carry the runoff from the city and drains it to the adjacent Ashley and Cooper Rivers. In this study, both DEM and DSM are tested to retrieve the physical properties of the distributed hydrologic and hydrodynamic model domains. The DSM is engaged for overland flow modeling so that the floodplain shows a more realistic flood propagation for CCF than using a high roughness factor and damping threshold. Given the high potential of CCF and tidal interconnection of the drainage network with adjacent rivers and the sea, the Charleston peninsula is an ideal test bed to test the fully-coupled modeling of the system facing CCF using the ICPR model.

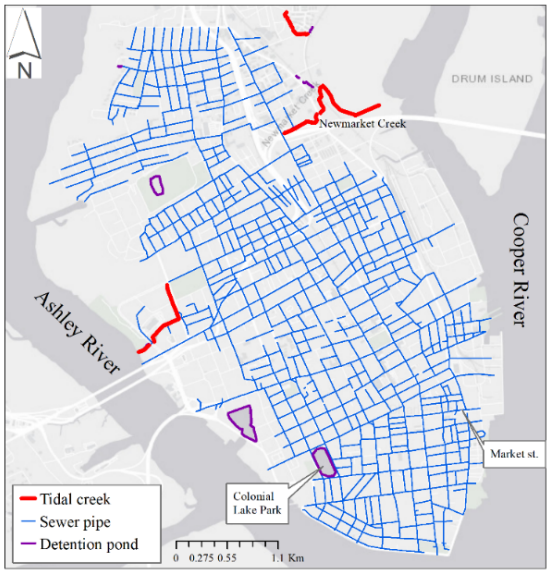

Fig. 3 The study area and the drainage system of the Charleston peninsula.

1. **Model setup**

The model setup process in ICPR for CCF modeling consists of several steps: 1) building 1D and 2D drainage networks, 2) incorporating topography models (DEM and DSM), 3) generating meshes for the study domain, 4) spatial and temporal model parameterization, 5) imposing model boundary conditions, and 6) developing the model coupling scheme. The underground pipes are considered as 1D conduits and the detention ponds are modeled as 1D floodwater storage nodes in the model. The tidal creeks and tidal wetlands are represented by 2D hydraulic elements in ICPR. The channel and pond routing systems are simulated using Saint-Venant equations. The overland flow models in ICPR are developed based on Energy balance, Momentum balance, and Diffusive wave equations (ICPR, 2021a). The spatially distributed land cover map and soil maps are gathered to generate hydrologic units' CNs for rainfall-runoff modeling. The land cover map is also used to define the roughness characteristics of the overland flow regions. The boundary conditions for the CCF models are 1) the spatially distributed rainfall and evapotranspiration information for determining the rainfall-runoff, and 2) the dynamic sea level or tide curve at downstream during the event, which is obtained from NOAA tide gauges' record. More details about the CCF model setup process are described in the following sections.

1. **Spatial and temporal data processing**

3.1.1 Drainage network

The drainage system of the Charleston peninsula consists of 4,718 pipes, 3 tidal channels, and a few coastal wetlands which surround the peninsula. The spatial layout and dimensions of the drainage network are obtained from CGA (2022). The underground pipes have mainly circular or rectangular cross-sections. The spatially distributed data and parameters are used to describe the physical characteristics of the drainage system, including topographic information from DEM and DSM (Table 1), stage-area, time-stage, and stage-volume curves, manning's roughness coefficients, and loss coefficient for entrance or exit loss. All model inputs are prepared in Arc-GIS environments as multipoint, polyline, and polygon features, and then they are imported into the ICPR model according to the required drainage features. In the ICPR model, underground sewer pipes are represented using 1D links, while the remaining open channel flow objects are represented by 2D links. When two or more pipes are connected at any location, the intersection is represented by a 1D node in ICPR. When 1D nodes interact with 2D overland flow, the momentum balance-based formulation is specified for switching energy and mass transport. Each node also requires inverted elevation data, which is obtained by subtracting the diameter of pipes and the freeboard from the ground elevation of the nodes.

The node type can be defined as stage-area, time-stage, or stage volume. The stage-area nodes determine the ponding depth and area based on the stage-area relationship in each node. The main purpose of using the stage-area nodes

is to represent the manholes. The time-stage node requires the time series of the tidal curves to specify the sea level conditions during the simulation period. The time-stage nodes represent the drainage outlets at the adjacent tidally influenced rivers. The stage-volume nodes determine the flood water storage or detention pond capacity based on the stage-volume curves, which are used for the representations of numerous detention ponds in the Charleston peninsula. The information associated with the stage-area and stage-volume curves is derived using DEM. Besides the sewer pipes, there are three tidal creeks and channels. The tidal creeks and channels are modeled as 2D links. The 2D links require the bathymetry of the channel for open channel flow simulation. The 2D links also need to specify the floodplain to switch from the channel flow to the overland flow and the tidal boundary conditions. For 2D links, the bathymetry information is extracted from the DEM. The floodplain topography is developed using the DSM which spatial data processing is detailed in Section 2.3.2.

Table 1: Sources of datasets acquired in this study

Data type	**Description**
Drainage network and Building rooftop	Drainage network, layouts and dimensions developed by Charleston
Land cover map and Soil Zone	National land cover map and gSSURGO soil grids
Rainfall data	Precipitation data of the rain gauges
Sea level	The tide level surrounding the Charleston peninsula
High Water Marks	Flood locations and flood depth recorded during the 2015 SC flood
Evapotranspiration	Daily mean evapotranspiration time series
DEM, DSM	LiDAR cloud points from the 3D elevation program

3.1.2 DEM and DSM processing

The DSM in the current study (Fig. 4) is generated using USGS LiDAR surveyed cloud points. The advantages of using the DSM for modeling the floodplain dynamics are 1) in urban areas, the flood propagation is controlled by terrain features mostly developed land use, and 2) the momentum balance-based overland flow modeling in ICPR takes into account the interaction between the flood water and developed structure for calculating the flood depth. Besides that, applying energy damping coefficients for urban structures allows energy blocking out of the buildings. On the other hand, the 1 m spatial resolution, LiDAR DEM (Table 1) information is used to extract 3D elevation of the tidal creeks, wetlands, and detention ponds, invert elevation of sewer pipes, natural slopes of 1D and 2D links, and basin slopes for honeycomb mesh. To process DSM, the LiDAR cloud points are retrieved from the USGS 3D elevation program (3DEP) (https://www.usgs.gov/3d-elevation-program, Table 1). The 3DEP mission uses LiDAR and Interferometric Synthetic Aperture Radar (IFSAR) technology to collect high-resolution elevation data for capturing a wide variety of topography in the USA. The DEM is retrieved for Charleston Penin-

sula with 1 m resolution (Fig. 5b and Table 2). The LiDAR dataset and DEM are projected into the NAVD88 coordination system to be consistent with NOAA sea level data. The LiDAR DSM of the Charleston peninsula is compiled by combining 16 USGS LiDAR scenes that contain approximately 167 million LiDAR points with eight different classes of Unassigned, Ground, Noise, Model Key/Reserved, Water, Rail, Bridge Deck, and High Noise. The Noise, Water, and High Noise cloud points are removed from the LiDAR cloud point dataset. In case of the presence of a multi-level flyover, the LiDAR points of DSM are quantified based on the ground elevation points. Finally, the sorted LiDAR cloud points are converted to a raster surface using the ArcGIS tool called 'LAS Dataset to Raster'. The inverse weighted distance, as a method of interpolation, and the natural neighbors' method, for filling up the void, are used to prepare the DSM. For merging each of the 16 LiDAR scenes, at first, they were converted from sorted LiDAR cloud points to a raster image. Then these raster datasets are all spatially joined and merged with each other using the 'Mosaicking tool' of ArcGIS to generate the DSM of the study area. The final DSM of the Charleston peninsula has a 0.5 m spatial resolution (Fig. 4).

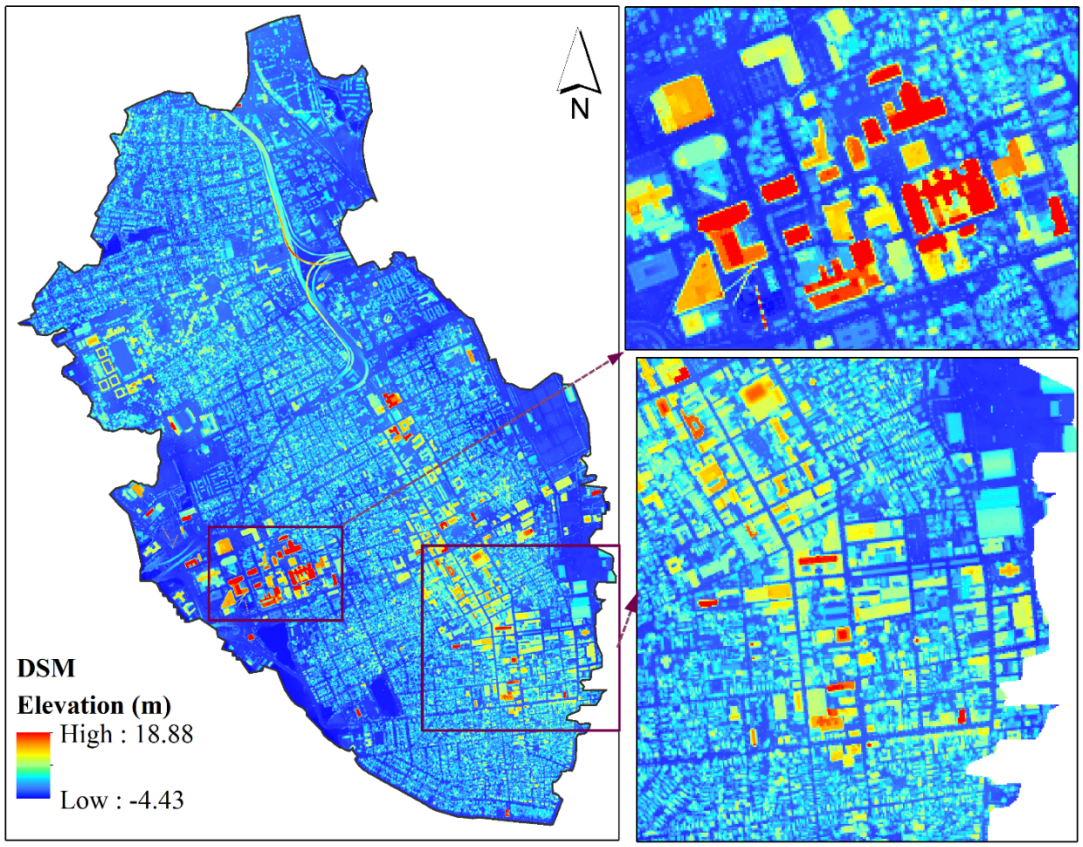

Fig. 4 The LiDAR Digital Surface Model of Charleston peninsula a) Location showing the Medical University

3.2 Mesh generation

Spatially flexible and unstructured meshes are employed to develop the fully-coupled CCF model. Triple-mesh configurations of honeycomb, TIN, and diamond meshes are required as previously shown in Fig. 1. The TIN mesh is used for surface hydraulics and has multiple advantages over a grid or cell-based 2D models as it has a flexible structure that can fit any complex topography. The ability to vary the spatial size of the TIN saves significant computational time by increasing the mech size in areas subjected to lower flood risk. The computational time can be reduced by coarsening TIN in areas with low-intensity development as well. The size of the mesh is also important for the ICPR for model stability. The 1D nodes and the vertices of TIN mesh (also known as 2D nodes in ICPR) of the drainage network are required to be set at the honeycomb (basin) mesh outlet such that those nodes collect the runoff from the honeycomb mesh as well as any receive backwater flow at tidally influenced nodes.

Since the mesh configuration depends on preservations of mass balance and energy/momentum balance, the formation of meshes for ICPR has been done through a trial-and-error approach. A tolerance limit (dz=0.001m) is set between two consecutive time steps for optimum mesh size generation to minimize the error from the energy and momentum balance. The model iteratively runs several times with the adopted mesh configuration and the mesh sizes are refined for that part of the study area that shows energy or momentum imbalance in the proceeding step.

Gravity-and-Froude-number-driven open channel flow highly depends on topography. Thus, an abrupt slope change can become a source of model error. To reduce the momentum and energy balance errors, the mesh size is refined using a 'breakpoint' or 'breakline' feature in dense urban areas and complex terrains. These two features, which facilitate a smooth transition of sudden changes in the mesh slope, can be automatically generated based on the region's physical characteristics. The breakpoint refines the TIN mesh at desired intervals or breakline captures the roadways or channel centerlines as a ridge line for vertices simplification (Saksena et al. 2019, 2021; Saksena *et al.*, 2020). The final mesh configuration accounts for the three different mesh types— with 19,444 honeycomb, 39,284 TIN, and 56,293 diamond meshes (Table 3).

3.3 Land cover and soil maps for model parameterization

The rainfall-runoff modeling of urbanized catchments using distributed hydrologic models at the parcel level is done following the NRCS-CN method. The NRCS-CN primary input parameters are land cover maps and soil groups. The 30 m resolution national land cover data has been used in the current study (Fig. 5a). In the current study, considering the highly urbanized areas of Charleston peninsula, the land cover map is updated with footprints of building rooftops by fusing the build-up areas in the national land cover datasets (Fig. 5a). The land cover of Charleston peninsula is classified with 10 land classes: barren land, buildings, deciduous forest, low intensity-developed area, medium intensity-developed area, high intensity-developed area, emergent herbaceous wetland, hay/pasture, waterbody, and shrub (Fig. 5a). Four soil groups from NRCS hydrologic map, respectively A, B, C, and D, are also used along with the land cover map to determine the CN (Table 2) for each pixel of the Charleston peninsula. In addition, two-dimensional overland flow characteristics depend on the roughness characteristics of the land cover. The same land cover maps for the distributed hydrologic model are also used to define the roughness characteristics of the overland flow area (Table 2). Therefore, the spatially distributed physical characteristics of floodplains for CCF modeling have four spatial attributes: 1) topography information, 2) CN, 3) Manning's roughness coefficient, and 4) soil types.

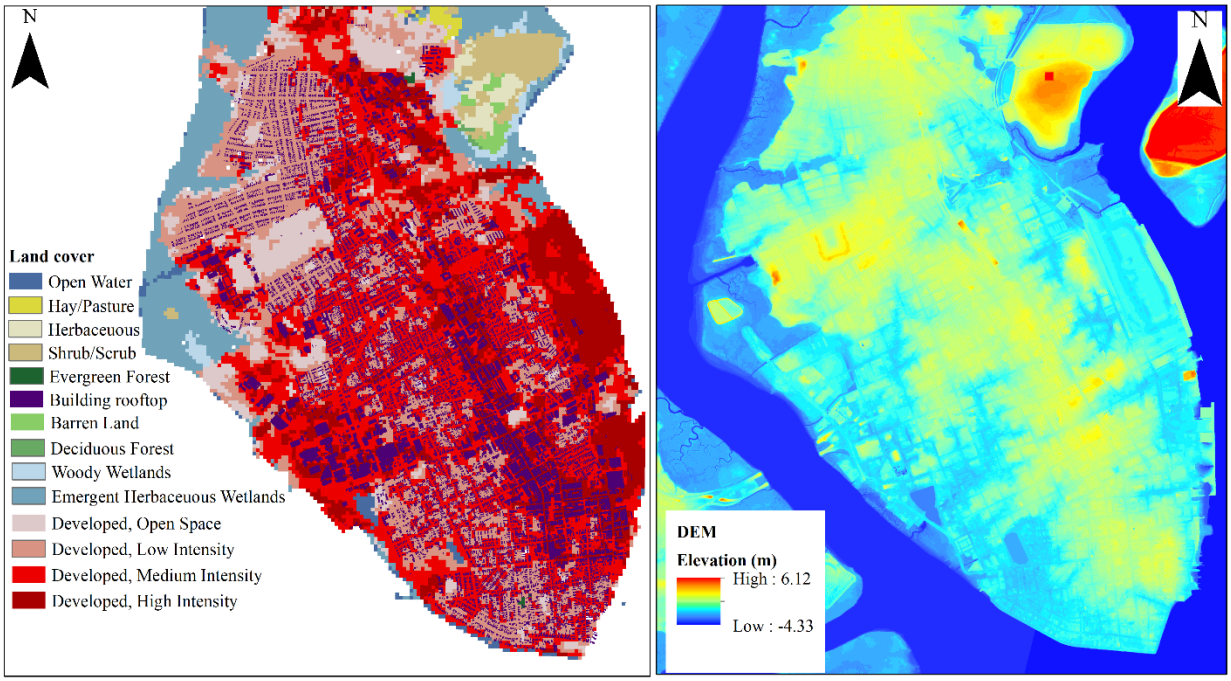

Fig. 5 a) Landcover map of Charleston peninsula b) Digital Elevation Models of Charleston peninsula

Table 2: Land use, CN, Manning's roughness in distributed hydrologic model

Land use type	**Manning's roughness coefficient**	**Curve numbers**		
	Shallow	Deep	Soil Zone-A	S
Barren Land	0.15	0.011	70	8
Building rooftops	1	1	100	1
Deciduous Forest	0.192	0.011	73	7
Developed, High Intensity	0.15	0.011	88	9
Developed, Low Intensity	0.1	0.011	81	8
Developed, Medium Intensity	0.08	0.011	84	8
Developed, Open Space	0.04	0.011	52	6
Emergent Herbaceous Wetlands	0.07	0.011	80	8
Evergreen Forest	0.16	0.011	77	7
Hay/Pasture	0.1	0.011	40	6
Herbaceous	0.035	0.011		6
Open Water	0.04	0.011	100	1
Shrub/Scrub	0.1	0.011		4
Woody Wetlands	0.4	0.4	86	8

3.4 Coupling in ICPR model

Hydrodynamics and distributed hydrologic models are integrated using a fully-coupled modeling framework, where spatiotemporally adaptive hydraulic time stepping is specified. The computation timestep requires two distinct terms: 1) the hydrology time step, which has a certain time increment to calculate the rainfall-runoff, and 2) the surface hydraulics time step, which dictates time intervals to keep up with the hydrology clock. Surface hydraulics time steps are often only a few fractions of a second long and it continues computation up to the next time interval of the hydrology time step. The time marching option in ICPR facilitates the coupling process. In ICPR, two-time marching options are available, Successive Approximation technique with Over-Relaxation (SOAR) and FIREBALL (ICPR, 2021a). The FIREBALL method is applied in this study because it is 2.5 to 30 times computationally faster than SOAR. For the FIREBALL approach, the minimum and maximum timesteps in time marching are specified as 0.01 and 5.12 seconds, respectively, based on the recommendation by Saksena et al. (2021). A maximum permitted timestep is established for each node, based on inflows, outflows, and available storage, to ensure that the changes in water level would not exceed the specified tolerance change in stage, which is chosen to prevent the mass-balance error. Likewise, the error in solving the continuity equation can be increased due to the initial model boundary conditions setup, if the node state remains dry. The initial model boundary conditions are set using a hot start file of the previous simulation. The hot start file defines the initial stage of all nodes and other model states.

Table 3: Description of final model configuration

@ >p(- 2) * >p(- 2) * @ **Computational elements** & **Quantity**
Model area (km^2) & 24.14
Number of 1-D hydraulic pipe links & 4822
Triangular mesh (2D node) & 39284
Honeycomb mesh (basin) & 19444
Diamond mesh (Overland flow zone & 56293
Types of hydraulic roughness zone & 14
Detention ponds & 3
Tidal creeks & 3
Surface hydraulics time step (s) & 0.6
Distributed hydrology time step (min) &

1.

3.5 Model sensitivity analysis, validation, and simulation events

The historical SC flood of 2015 in the Charleston peninsula is considered in this study for the simulation of CCF. This event brought rainfall with a return period of about 1,000 years. Different combinations of model parameters and

configurations are tested for sensitivity analysis, including two different topography models (DEM or DSM) for floodplain, changes in ELF, and using three overland flow estimation methods, i.e., energy balance, momentum balance, and diffusive waves. The ELF varies between 0.4 to 1 and it is chosen as the main calibration parameter. A total of 42 model configurations are tested to achieve the highest possible modeling accuracy. The best-performed model was achieved by finding the optimum value of ELF under different terrain models and overland flow estimation methods. The simulated flood depth was validated against the USGS high water marks (HWM) observation and SCDOT road closure reports during the SC flood event of 2015. The calibration results are compared using a Taylor diagram to sort out the best-fit model parameters. The Taylor diagram represents the correlation coefficient, standard deviation (SD), and the root mean squared diagram in a single plot to show the relative accuracy of multiple models. In addition to the SC Flood event of 2015, a nuisance flood event, in Nov 2021, was chosen to asse the performance of CCF model to represent high tide flooding. The Nov 2021 king tide caused a nuisance flood, when 5 road closures were reported. The flood event is named hereafter as 'tidal flood 2021'. This investigation is important to identify the tidally influenced prone areas in the Charleston peninsula. The simulations run on a machine with the intel core i7-9700 CPU and by activating all threads of the CPU for parallel processing. The typical run time takes about 4.5-5 hours for a single event simulation.

4. Results

4.1 Sensitivity analysis

4.1.1 Effects of topography model

The CCF modeling performance is assessed by changing the topography models between DEM and DSM. The performance of the DEM and DSM in model simulation is shown in Fig. 6, where the Taylor diagram, along the - direction shows the correlation coefficient of different model performances and along the radial axes the standard deviation (SD) of the simulated flood depth in comparison with the observed HWMs. The Root Mean Squared Error (RMSE) in the Taylor diagram is proportional to the distance between the observed points to the model simulated values (Fig. 6). The relative accuracy among the compared models are high for those models which are closer to the observed points in the Taylor diagram. The CCF model is found highly sensitive to the terrain model (Fig. 6). Using DSM as terrain model results in a better performance than using DEM. The Taylor diagram shows the accuracy of elevation data can significantly improve the model performance. The simulated inundation depth using DSM has achieved a maximum correlation coefficient of 0.82 while using DEM based CCF model the best performance is measured by a maximum correlation coefficient of 0.6. In other words, the accuracy of CCF modeling can be improved by up to 15-33% using the DSM. In a fully-coupled model the inaccuracy of DEM data in simulating CCF can be potentially caused by two main reasons, 1) DEM underestimates the floodplain topography, particularly the elevation of developed structures as they are neglected in the DEM

model, and 2) the tidal flood propagation from surrounding rivers has changed its route due to neglection of the height of the structures in DEM. Further, the inaccuracies in DEM or DSM could be stemmed from an underestimation of the missing elevation points to generate the topography model. This is aligned with the finding of other researchers as raster surface interpolation may result in the inaccuracy of flood depth calculation since the overland flow estimation, particularly spatial nonstationarity may present in the surface interpolation method (Karamouz and Fereshtehpour 2019).

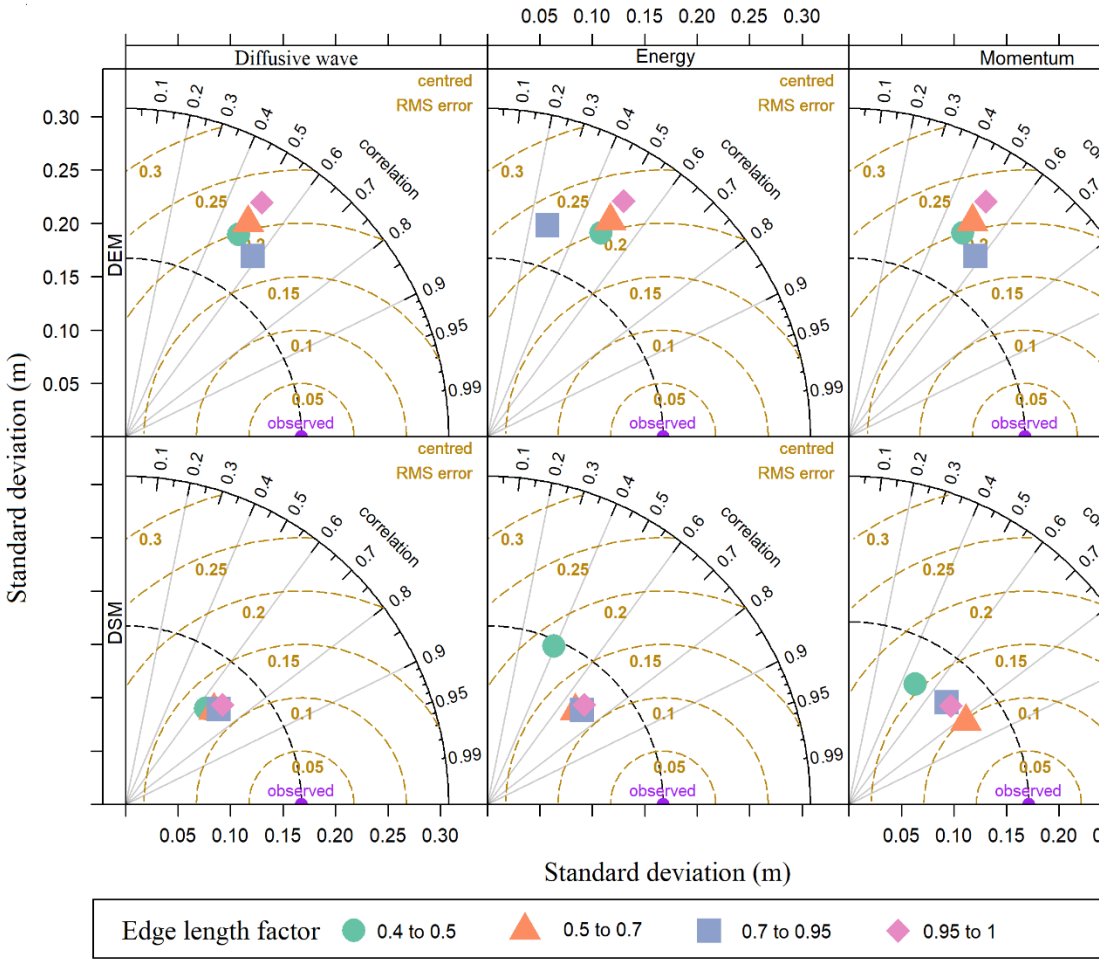

@ >p(- 0) * @

Fig. 6 Taylor diagram for sensitivity analysis of model performance with the model formulation, elevation model, and edge length factor

4.1.2 Sensitivity of overland flow model formulation

The performance of energy balance, momentum balance, and diffusive wave method for overland flow calculation are tested in the second cohort of sensitivity analysis to improve the model performance in simulating the 2015 CCF FIM and flood depth. The model performance is compared using the Taylor diagram (Fig. 6). The relative model performance ranked from momentum balance, diffusive wave, and energy balance method for overland flow simulation. The tidally influenced areas in momentum balance are more representative than the diffusive wave method since the later method neglects the inertia terms, such as the local acceleration. A total of 42 model tests and their associated performances are summarized in Fig. 6. When the ELF increases, the time to peak in flood hydrograph speeds up. Consequently, the flood model with high ELF shows relatively higher ponding depth and a faster flood peak. The standard deviation of the simulated flood depth using DEM is relatively higher than DSM. The urban watershed has a relatively higher and faster flood peak that may support a high ELF. However, the model performance with an ELF closer to 1 results in a high ponding depth that overestimates the flood depth. On the other hand, an ELF closer to 0.4 underestimates the observed flood depth. The ELF between 0.5 to 0.7 shows a reasonable estimate to get a good CCF model performance. Among the overland flow calculation methods, the momentum-based approach results in the best accuracy.

These findings suggest that accurate quantification of the velocity in the floodplain may result in a better CCF model performance. The model sensitivity analysis showed that an ELF ranging between 0.6 to 0.7 with momentum balance-based formulation and using DSM for topography representation would be optimal for CCF modeling. The highest correlation coefficient between the simulated flood depth and USGS HWM is achieved at 0.86, as a result of adopting the momentum balance method with an ELF of 0.7. Moreover, because 2D shallow water equations are more convective acceleration conservative they can improve CCF dynamics, which also has prominent advantages in areas with complex floodplains.

4.2 Validation results

The sensitivity analysis of CCF modeling suggested that the model configurations with the use of DSM, momentum-based overland flow formulation, and ELF of 0.7. This configuration is further used for the model against road closure reports from SCDOT. During the tidal flooding event, (Fig. 7b), Charleston experienced a 1.65m NAVD high tide. The king tide is reported by NOAA to be the tenth-highest tide recorded in Charleston harbor. About 5 locations, marked in Fig. 7b, experienced widespread high tide flooding in the Charleston peninsula, including Morrison drive and part of America Street (Fig. 7b) . The dynamic sea level boundary condition, has been applied to improve the tidal flood distribution, to identify the submerged drainage outlets and the low-lying areas in coastal peninsula boundaries. The representation of the coastal watersheds exposed areas to tidally influenced rivers or sea in 1D models is limited

to drainage outlets. Most 1D models (e.g. SWMM) account for the tidally influenced nodes and links which are mostly the submerged outlets, and not other tidally influenced parts like tidal wetlands (Tanim and Goharian 2020b). However, in the current study, and in order to address this issue, the exposures of the coastal watershed to tidally influenced rivers and the sea is represented using continuous land-sea boundary along with setting up a dynamic sea level as boundary condition conditions.

Fig. 7a shows the affected areas by the 2015 SC flood. Similar places are also marked in Fig. 7b, during the SC flood of 2015. The marked flooded streets in Fig. 7b are the primary concerns from CCF simulations since the rainfall-induced flood can further exacerbate the flooding issue in these areas. Apparently, the flood problem in 2015 was more widespread than during the 2021 tidal floods, since it was associated with compounding effects and tidal flow reduced drainage capacity to carry more storm runoff through the sewer systems. Table 4 shows the model precision for predicting the actual flooded areas during these two events. The efficiency of the CCF model in capturing street-level floods is found 98.35% and 100% for SC 2015 flood and 2021 tidal flood events, respectively (Table 4).

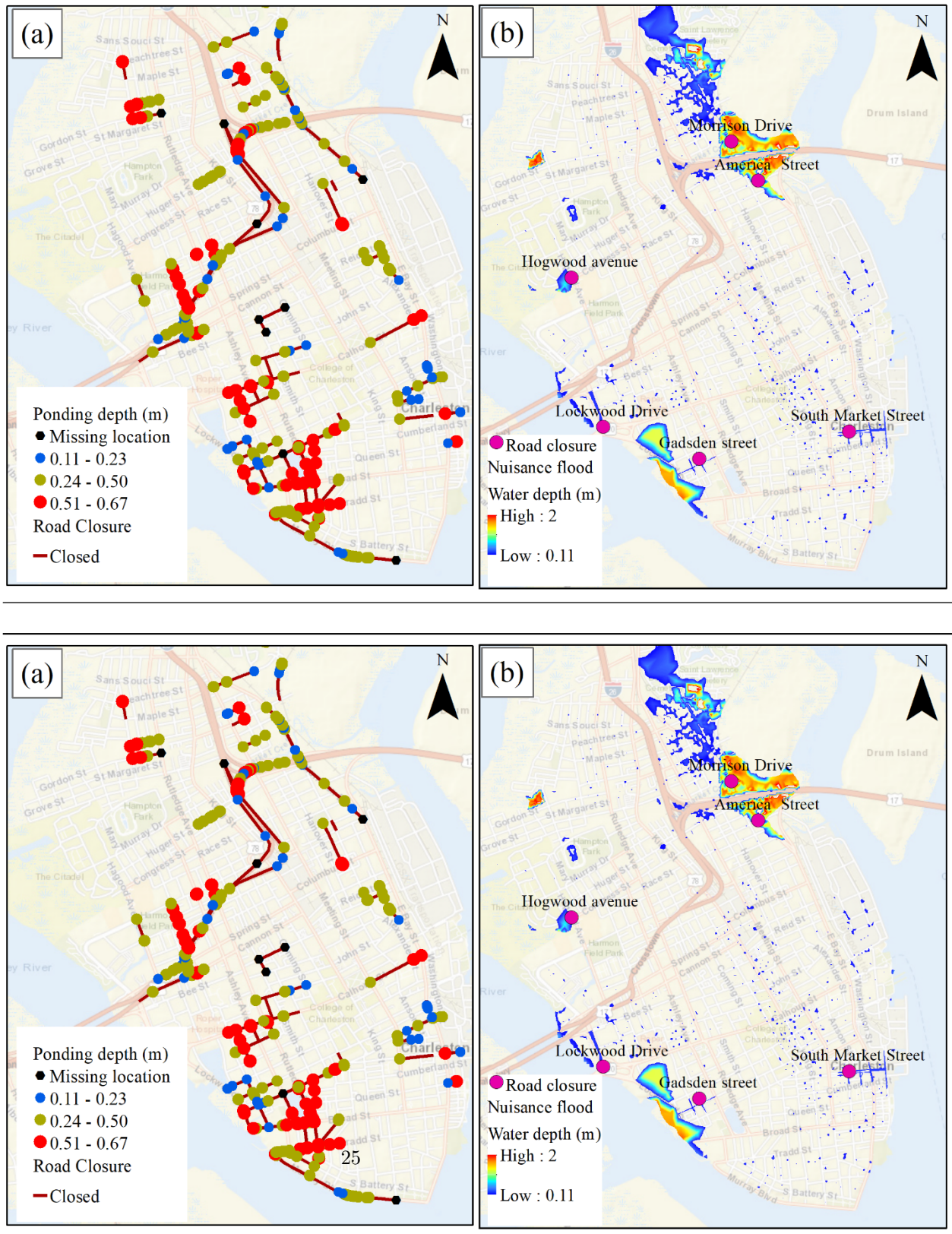

Fig. 7 The validation of ICPR model results with a) SCDOT road closure data during SC flood event 2015, b

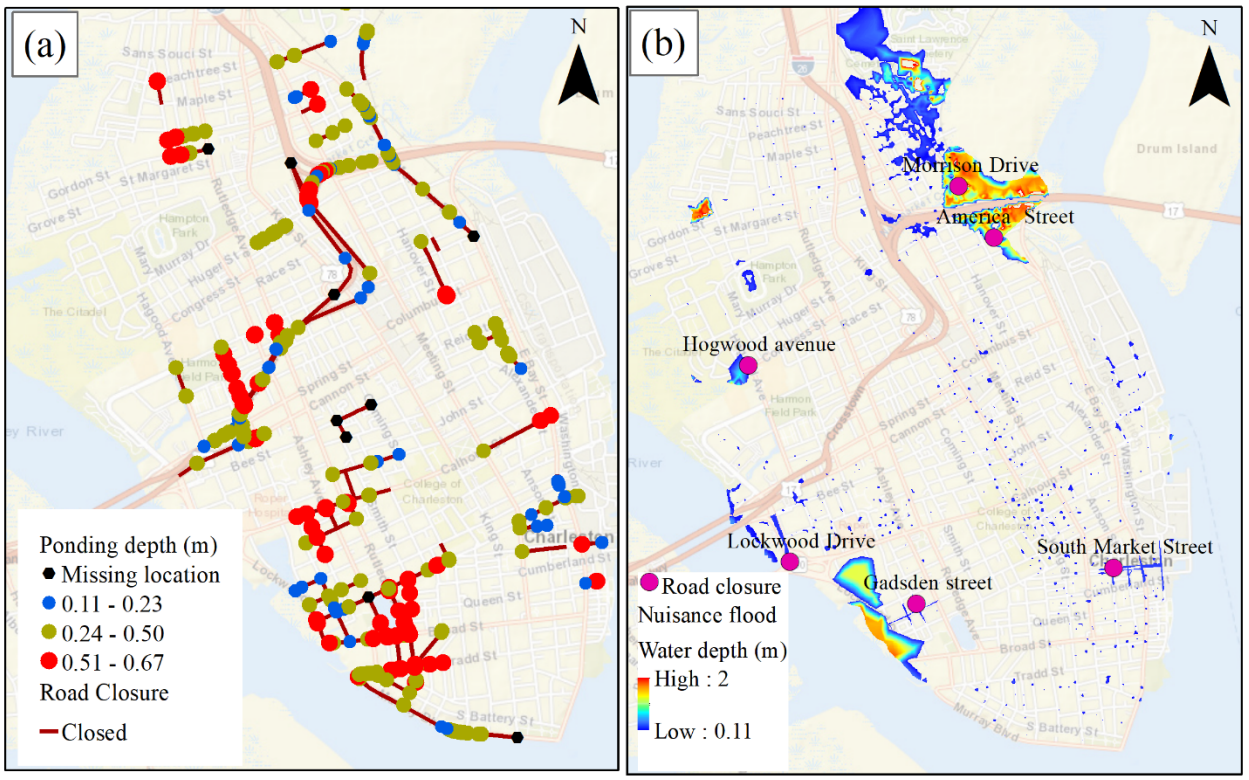

Table 4: Summary of model precision based on validation events

Flood events	Total road closure locations2	Model-detected flood locations	No. of missing loc
SC Flood event 2015	547	538	9
Nuisance flood 2021	5	5	0

[1]Road closure data is reported by SCDOT

[2] Model efficiency $= \frac{\text{Sum of model detected road closures}}{\text{Total reported road closures}}$

4.3 SC CCF event 2015 simulation

The simulated flood scenario during the SC flood event 2015 is shown in Fig. 8. The pixel's colors correspond to 5 inundation depth levels (Fig. 8a-8c). Three distinct scenarios are further extracted from this flood simulation to analyze flood depth during this event:

- Scenario-A. peak flood after the first rainfall event with a low tide condition (Fig. 8a),

- Scenario-B. simultaneous high rainfall peak and high tide (Fig. 8b), and
- Scenario-C. rainfall-induced peak flood occurs after attenuation of tidal influence (Fig. 8c).

Fig. 8b shows the CCF conditions (Scenario-B) when the drainage outlets and surrounding tidal creeks of the Charleston peninsula are occupied with tidewater. Low-lying tidal creeks are found inundated during the peak flood condition; these areas contribute to worsening the flood conditions. The effect of the tide in CCF is prominent by comparing scenarios B with C (Figures 8b and 8c). The results show that the flood risk, caused by CCF, surpassed the flood risk caused solely by intense rainfall.

Simulation results show a significant increase in ponding depth 0.41-0.67 m under the CCF condition (Scenario-B) than the rainfall-derived flood (Scenario-C). The flood inundation extent (Fig. 8b, Scenario-B) during the simultaneous peak rainfall and high tide condition is 19% greater flood extent under Scenario-C (Fig. 8c). Therefore, the joint occurrences of rainfall peak and the high tide offer the highest flood risk. However, the Scenario-C flood map (Fig. 8c) reveals that some inland locations (Charleston harbor) have higher flood depth than Scenario-B (Fig. 8b). This is mainly due to the discharge of flood water from the adjacent tidal creeks and tidally impacted flooded area (tidal creeks in Fig, 8c) to these locations, as the flood depth in the rainfall-tidal transition zone is reduced.

Charleston has a well-engineered drainage network that covers nearly the whole peninsula. The tidewater propagates to the low-lying area drainage system since the waterway has a shorter travel time with tide changes. Fig. 9 shows the maximum time-independent flood depth at each pixel during the flood event regardless of the rainfall amount and tide level conditions. Overall, the detention ponds in the Charleston peninsula provide a decent functionality for capturing floodwater. Some detention ponds (Colonial Lake Park) are also connected with tidal creeks and wetlands, and therefore, receive less storm runoff. The peripheral part of the Charleston peninsula, shown in Fig. 8b, presents higher ponding depth than other places under Scenario-B due to the tidal influence. On the other hand, the central part of the peninsula is more prone to rainfall-derived flooding (Scenario-C and Fig. 8c).

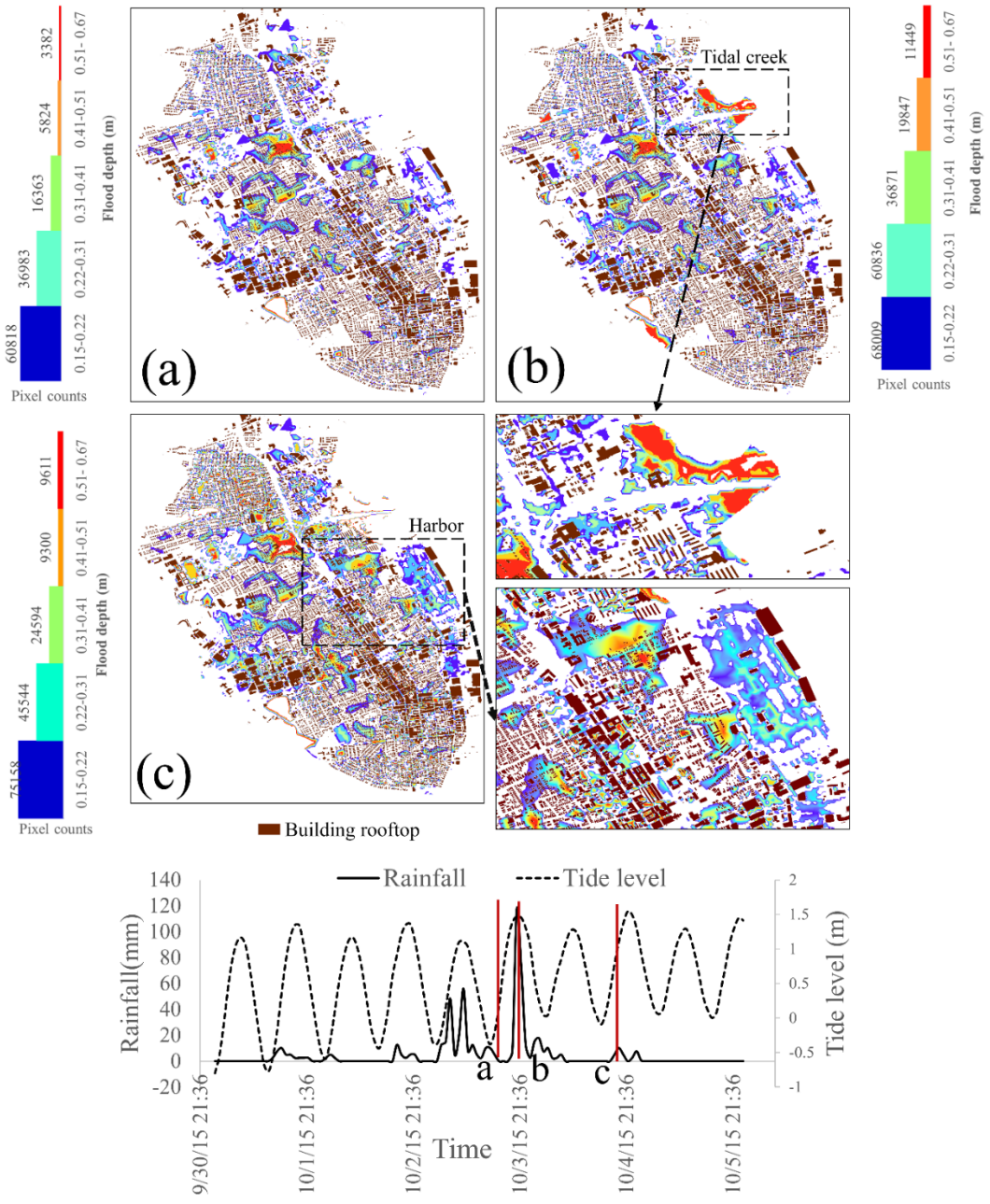

Fig. 8 Flood depth during the SC flood of 2015 and the rainfall-tide hydrograph during the flood event. a) T

The simulated maximum time-independent flood depth during the SC 2015 flood is shown in Fig. 9. The ponding depth over several junctions in the sewer system reaches up to 0.67 m. The flood risk right above the upstream of Newmarket creeks (Fig. 9a) is higher than in any other place. This can be attributed to the presence of three tidal creeks adjacent to this location, which causes the backwater from high tide and rainfall-runoff to combine and produce higher ponding depth at this location (Fig. 9a).

During high tide flooding, coastal water overflows from the tidal wetlands and cause drainage outlet to be submerged in adjacent tidal rivers. For instance, the floodwater in North market street has a significant tidal influence while the storm runoff is supposed to be drained. Besides the ponded nodes, some open spaces are flooded because storm runoff accumulates in these areas, and ponding of floodwater happens after runoff drains from the highly urbanized areas.

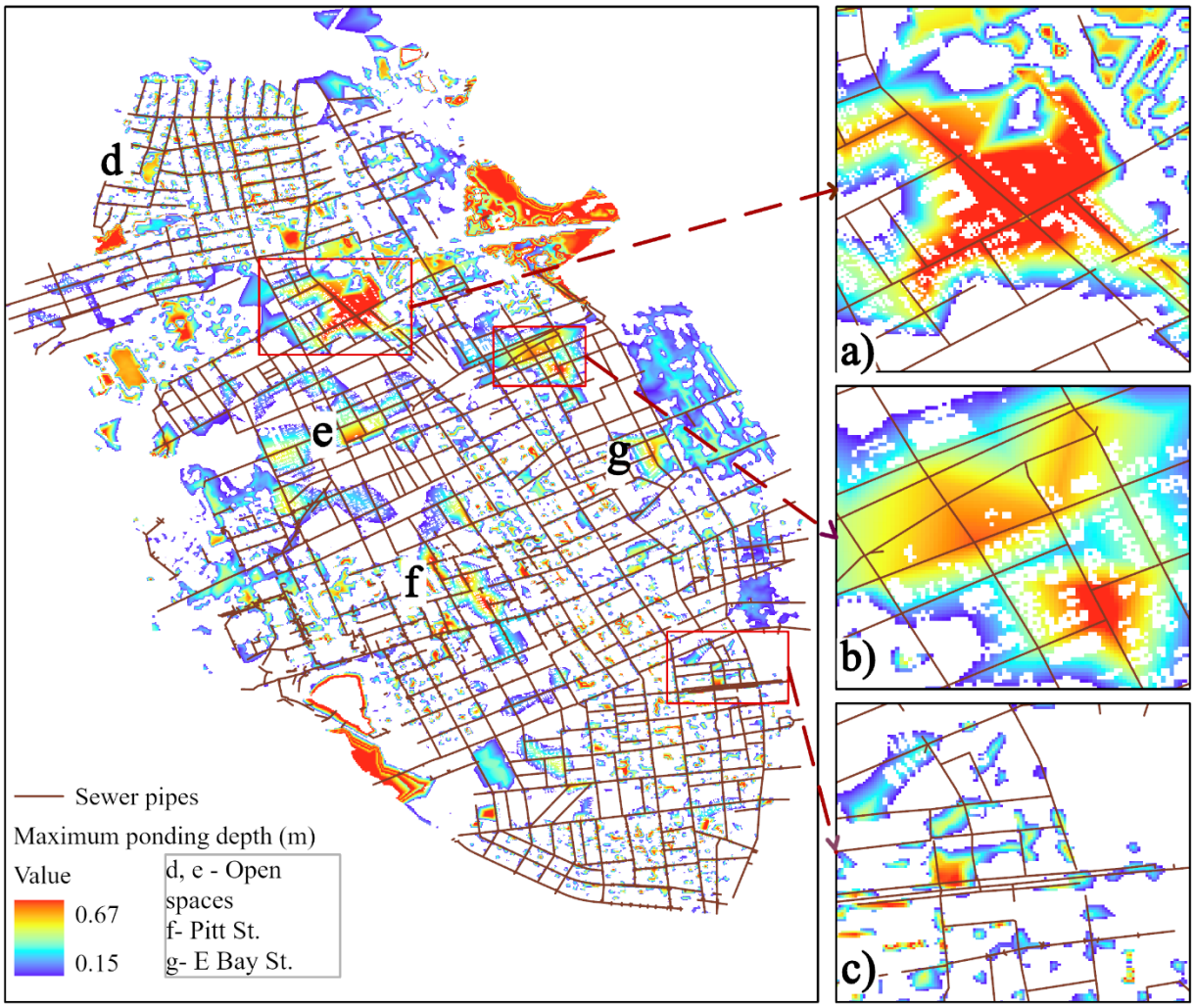

Fig. 9 Simulated maximum ponding depth throughout the SC flood of 2015 in the ICPR model. The zoom-in

In fact, Fig. 9a, 9b, and 9c shades light on various existing flood issues in different parts of the Charleston peninsula. In general, tidal floods pose a growing threat to this historic town and neighborhoods. For example, the severity of the flooding at the American street intersections and at South Market Street are prominent (see Fig. 7b and 9c). Moreover, the highlighted area in Fig 9a is located just above the Newmarket tidal creek, where ICPR predicts higher flood risk because of the coarse mesh size. The frequent nuisance flood problem in these locations is an early warning of sea level rise, which in turn affects the number and magnitude of tidal flooding in the Charleston peninsula in the future.

The number of high tide sunny day flooding is expected to rise up to 180 days per year by 2045 in Charleston (Morris and Renken, 2020). Some residential areas are more prone to nuisance flooding. It is suggested these neighborhoods elevate their ground floor by about 0.5 m to cope with the current flooding situation. Besides that, some places, such as those marked in Fig. 9 with the alphabets d and e (open space), f (Pitt St.), and g (E Bay St.) are predominantly flooded with rainfall alone, and without any tidal influence. In future studies, the CCF flood simulation integrating with climate change projections and sea level rise scenarios is needed to propose mid to long-term flood resilience plans in these areas.

1. **Results Discussion**

Previous research efforts for CCF modeling in the Charleston peninsula have engaged nuisance flood models (e.g., Morris and Renken, 2020) or DEM-based empirical rainfall-runoff models (e.g., Conrad, 2019). This study improves the flood risk analysis for the Charleston peninsula applying a fully-coupled model that integrates the complex drainage system with a distributed hydrologic model. In this study, the distributed rainfall-runoff model is parameterized with fine-resolution CNs. The floodplain dynamics and floodwater propagation representations are improved by including the urban structures in three ways, 1) the building footprints are imposed in NLCD land use maps, 2) the damping threshold is applied in the area with building rooftops, 3) the elevation from DSM is incorporated in the floodplain characterization. In the case of DSM data unavailability, the CCF model can be developed using DEM and applying energy damping threshold at areas of developed structures. This technique can be further improved for floodplain modeling by accounting for the energy damping for structures. This leads to higher capacity in calculating the rain-on-grid of the urbanized coastal watersheds. The CCF model captures the physical process more holistically and results show that Charleston is suffering from the tidal influence and sewer system congestion at several places.

A vast majority of the Charleston peninsula is urbanized by landfilling the tidal creeks which increases the risk of flooding in the low-lying peninsula. The nuisance flooding is frequent and can occur any time when the tide level exceeds 1.17m NAVD tide level (Morris and Renken, 2020). CCF management in the peninsula necessitates immediate attention since the tidal flows significantly reduce the drainage capacity. This study found that the flood risk in South and North Market St., American street near Morrison St., Gadsden creek, and Lockwood drive is higher and need more attention on tidal flood management. The neighborhoods near Colonial Lake, and Gadsden Creek requires improved flood resilience and preparation to protect those historical places from sea level rise and ongoing nuisance flooding. The northern part of the Charleston peninsula has higher flood susceptibility due to heavy rainfall. The southern parts, on the other hand, pose a higher susceptibility due to tidal flooding and low-lying elevation. The ponding caused by the storm runoff calls for the development of smart real-time drainage systems in face of CCF.

1. Summary and Conclusions

The CCF has a destructive potential in coastal urban areas. Over the past decades, several CCF models have been developed. However, the flood dynamics in the coastal urban area are still not well understood since these models deploy a one-way or two-way coupling procedure. In this study, a drainage system consisting of tidal creeks and underground sewers having 1D and 2D modeling characteristics is adopted. Moreover, the underground drainage network is modeled using 1D links, and tidal channels are modeled by 2D hydraulic elements. In a one-way coupling system, 1D hydraulics ignores the coastal flood-induced overland flow in tidal channels (Shi et al. 2022). The tidally influenced drainage system in simulating CCF should be explicitly considered rather than one-way or two-way coupling. In a fully-coupled system, however, the underlying connected and dynamic physics of CCF are incorporated by representing the interconnection of tidal flow with the surface runoff in each time step and model nodes, which in turn makes the CCF models truly process-oriented. The proposed fully coupling framework for CCF modeling considers the mass balance of the CCF process and presents a novel solution to eliminate these issues with one-way, two-way, or tightly coupling systems and offers flexibility to incorporate a wide-variety of drainage components in coastal watersheds.

In the current study, a fully-coupled CCF model is developed coupling the distributed hydrologic model and surface hydraulics (1D and 2D). This CCF model is the first attempt to establish a fully-coupled CCF model to find FIMs for the Charleston peninsula as well. The CCF model considers the mass balance of process-oriented CCF caused by joint storm surge and rainfall runoff interactions. The drainage network consists of underground sewer pipes (1D links), and tidal channels (2D links), and the detention ponds can represent the interconnection of storm runoff with tides. The overland flow model considers the tidal backwater flow from surrounding tidal rivers. The ELF has been applied to calibrate the CCF model. Results show that using DSM to represent the topography and momentum balance method as an overland flow model with an ELF of 0.7 yields the most accurate flood simulation results with a correlation coefficient of 0.86. The momentum balance method achieves the highest accuracy since the physics of floodwater interactions with urban structures is represented rather conservatively in momentum balance compared to energy balance or diffusive wave methods. The flood simulation shows that both the drainage outlets and riverbanks overflowed by high tides can make significant flooding conditions in Charleston. The CCF model helps to identify both tidally influenced flood locations and rainfall-influenced flood locations. The CCF during simultaneous intense rainfall and the high tide suggests the highest flooding risk, about 19% greater flood inundation extent than the flood caused by rainfall alone. The validation with road closure data proves the model's capacity to capture street-level flooding. The model validation result shows that the CCF model captures 98.35% of road closure locations in the SC flood event of 2015.

While the proposed fully-coupled modeling effort in this study offers a great

leap forward for the flood modeling community and also for flood engineers and managers, in particular in the Charleston region, future studies should target increasing the computation power of the modeling to make this model more operational. Moreover, it is expected that further studies to be conducted for testing and validating the momentum-balance-based overland-flow models with observed flood velocity data or sensors-based observation rather than flood depth to improve micro-level-modeling physics. Additionally, a flood optimization ICPR method for using a spatially flexible ELF can be recommended in order to improve the efficacy of CCF modeling.

1. **Data Availability**

The input data and optimal model parameter used for developing the ICPR model in the study will (data archiving is underway) be available at the University of South Carolina via Open Science Framework (OSF). OSF allows researchers to collaborate, document, archive, share, and register research projects, materials, and data.

References

Bevacqua, E. *et al.* (2019) 'Higher probability of compound flooding from precipitation and storm surge in Europe under anthropogenic climate change', *Science Advances*, 5(9), p. eaaw5531. doi: 10.1126/sciadv.aaw5531.Bevacqua, E. *et al.* (2020) 'Brief communication: The role of using precipitation or river discharge data when assessing global coastal compound flooding', *Natural Hazards and Earth System Sciences*. Copernicus GmbH, 20(6), pp. 1765–1782.Bilskie, M. V and Hagen, S. C. (2018) 'Defining flood zone transitions in low-gradient coastal regions', *Geophysical Research Letters*. Wiley Online Library, 45(6), pp. 2761–2770.Čepienė, E. *et al.* (2022) 'Sea Level Rise Impact on Compound Coastal River Flood Risk in Klaipėda City (Baltic Coast, Lithuania)', *Water* . doi: 10.3390/w14030414.CGA 2022. Charleston Government Authority geospatial data archive. Available at. https://www.charleston-sc.gov/. Accessed on 02/10/2021Conrad, C. D. (2019) *The Use of an L-Thia Based Modified Curve Number Runoff Model for Flood Hazard Mapping in Charleston, South Carolina*, *Theses*. College of Charleston. Available at: https://login.pallas2.tcl.sc.edu/login?url=https://www.proquest.com/dissertations-theses/use-l-thia-based-modified-curve-number-runoff/docview/2378961714/se-2?accountid=13965.Hunter, N. M. *et al.* (2008) 'Benchmarking 2D hydraulic models for urban flooding', in *Proceedings of the Institution of Civil Engineers-Water Management*, pp. 13–30.ICPR (2021a) *ICPR4 Technical Reference Manual*, *ICPR4 Technical Reference Manual*. Winter Springs, Florida: Streamline Technologies Inc.,. Available at: www.streamnologies.com/misc/ICPR4_DOCS.zip.ICPR (2021b) *ICPR4 Validation Report*, *ICPR4 Validation Report*. Winter Springs, Florida: Streamline Technologies Inc.,. Available at: www.streamnologies.com/misc/ICPR4_DOCS.zip.Ikeuchi, H. *et al.* (2017) 'Compound simulation of fluvial floods and storm surges in a global coupled river-coast flood model: Model development and its application to 2007 Cyclone Sidr in Bangladesh', *Jour-*

nal of Advances in Modeling Earth Systems, 9(4), pp. 1847–1862. doi: https://doi.org/10.1002/2017MS000943.Jafarzadegan, K. *et al.* (2021) 'Toward Improved River Boundary Conditioning for Simulation of Extreme Floods', *Advances in Water Resources*, p. 104059. doi: https://doi.org/10.1016/j.advwatres.2021.104059.Jang, J.-H. and Chang, T.-H. (2022) 'Flood risk estimation under the compound influence of rainfall and tide', *Journal of Hydrology*, 606, p. 127446. doi: https://doi.org/10.1016/j.jhydrol.2022.127446.Joyce, J. *et al.* (2018) 'Cascade impact of hurricane movement, storm tidal surge, sea level rise and precipitation variability on flood assessment in a coastal urban watershed', *Climate Dynamics*, 51(1), pp. 383–409. doi: 10.1007/s00382-017-3930-4.Karamouz, M. *et al.* (2017) 'Integration of inland and coastal storms for flood hazard assessment using a distributed hydrologic model', *Environmental Earth Sciences*. Springer, 76(11), pp. 1–17.Karamouz, M. and Fereshtehpour, M. (2019) 'Modeling DEM Errors in Coastal Flood Inundation and Damages: A Spatial Nonstationary Approach', *Water Resources Research*, 55(8), pp. 6606–6624. doi: https://doi.org/10.1029/2018WR024562.Kuchment, L. S. and Gelfan, A. N. (2002) 'Estimation of extreme flood characteristics using physically based models of runoff generation and stochastic meteorological inputs', *Water International*. Taylor \& Francis, 27(1), pp. 77–86.Kupfer, S. *et al.* (2022) 'Investigating the interaction of waves and river discharge during compound flooding at Breede Estuary, South Africa', *Natural Hazards and Earth System Sciences*, 22(1), pp. 187–205. doi: 10.5194/nhess-22-187-2022.Leander, R. and Buishand, T. A. (2007) 'Resampling of regional climate model output for the simulation of extreme river flows', *Journal of Hydrology*. Elsevier, 332(3–4), pp. 487–496.Mishra, S. K., Gajbhiye, S. and Pandey, A. (2013) 'Estimation of design runoff curve numbers for Narmada watersheds (India)', *Journal of Applied Water Engineering and Research*. Taylor \& Francis, 1(1), pp. 69–79.Morris, J. T. and Renken, K. A. (2020) 'Past, present, and future nuisance flooding on the Charleston peninsula', *PLOS ONE*. Public Library of Science, 15(9), pp. 1–16. doi: 10.1371/journal.pone.0238770.Muñoz, D. F. *et al.* (2021) 'From local to regional compound flood mapping with deep learning and data fusion techniques', *Science of The Total Environment*, 782, p. 146927. doi: https://doi.org/10.1016/j.scitotenv.2021.146927.Muñoz, D. F. *et al.* (2022) 'Accounting for uncertainties in compound flood hazard assessment: The value of data assimilation', *Coastal Engineering*, 171, p. 104057. doi: https://doi.org/10.1016/j.coastaleng.2021.104057.Navid, T. *et al.* (2022) 'Quantification of Compound Flooding over Roadway Network during Extreme Events for Planning Emergency Operations', *Natural Hazards Review*. American Society of Civil Engineers, 23(2), p. 4021067. doi: 10.1061/(ASCE)NH.1527-6996.0000524.NRC (1994) *Hurricane Hugo, Puerto Rico, the Virgin Islands, and Charleston, South Carolina, September 17-22, 1989*. Edited by National Research Council. National Academies Press.Paquet, E. *et al.* (2013) 'The SCHADEX method: A semi-continuous rainfall--runoff simulation for extreme flood estimation', *Journal of Hydrology*. Elsevier, 495, pp. 23–37.Pasquier, U. *et al.* (2019) 'An integrated 1D–2D hydraulic modelling approach to assess the sensitivity of a coastal region to compound flooding hazard under climate

change', *Natural Hazards*, 98(3), pp. 915–937. doi: 10.1007/s11069-018-3462-1.Saksena, S. *et al.* (2020) 'A Computationally Efficient and Physically Based Approach for Urban Flood Modeling Using a Flexible Spatiotemporal Structure', *Water Resources Research*, 56(1), p. e2019WR025769. doi: 10.1029/2019WR025769.Saksena, S., Merwade, V. and Singhofen, P. J. (2019) 'Flood inundation modeling and mapping by integrating surface and subsurface hydrology with river hydrodynamics', *Journal of Hydrology*, 575, pp. 1155–1177. doi: https://doi.org/10.1016/j.jhydrol.2019.06.024.Saksena, S., Merwade, V. and Singhofen, P. J. (2021) 'An Alternative Approach for Improving Prediction of Integrated Hydrologic-Hydraulic Models by Assessing the Impact of Intrinsic Spatial Scales', *Water Resources Research*, 57(10), p. e2020WR027702. doi: https://doi.org/10.1029/2020WR027702.Sanders, B. F. *et al.* (2020) 'Collaborative Modeling With Fine-Resolution Data Enhances Flood Awareness, Minimizes Differences in Flood Perception, and Produces Actionable Flood Maps', *Earth's Future*, 8(1), p. e2019EF001391. doi: https://doi.org/10.1029/2019EF001391.Santiago-Collazo, F. L., Bilskie, M. V and Hagen, S. C. (2019) 'A comprehensive review of compound inundation models in low-gradient coastal watersheds', *Environmental Modelling & Software*, 119, pp. 166–181. doi: https://doi.org/10.1016/j.envsoft.2019.06.002.Shen, Y. *et al.* (2019) 'Flood risk assessment and increased resilience for coastal urban watersheds under the combined impact of storm tide and heavy rainfall', *Journal of Hydrology*, 579, p. 124159. doi: https://doi.org/10.1016/j.jhydrol.2019.124159.Shi, S., Yang, B. and Jiang, W. (2022) 'Numerical simulations of compound flooding caused by storm surge and heavy rain with the presence of urban drainage system, coastal dam and tide gates: A case study of Xiangshan, China', *Coastal Engineering*, 172, p. 104064. doi: https://doi.org/10.1016/j.coastaleng.2021.104064.Tang, H. S. *et al.* (2013) 'Vulnerability of population and transportation infrastructure at the east bank of Delaware Bay due to coastal flooding in sea-level rise conditions', *Natural Hazards*, 69(1), pp. 141–163. doi: 10.1007/s11069-013-0691-1.Tanim, A. H. and Goharian, E. (2020a) 'Developing a hybrid modeling and multivariate analysis framework for storm surge and runoff interactions in urban coastal flooding', *Journal of Hydrology*, p. 125670. doi: https://doi.org/10.1016/j.jhydrol.2020.125670.Tanim, A. H. and Goharian, E. (2020b) 'Hybrid Modeling Framework for Simulating Compound Floods in a Coastal City', *World Environmental and Water Resources Congress 2020*. Reston, VA: American Society of Civil Engineers, pp. 218–228. doi: 10.1061/9780784482964.022.USACE (2020) *Charleston Peninsula, South Carolina: A Coastal Flood Risk Management study Draft Feasibility Report/ Environmental Assessment*. Charleston, SC. Available at: https://www.sac.usace.army.mil/Missions/Civil-Works/Supplemental-Funding/Charleston-Peninsula-Study/.Walega, A. *et al.* (2020) 'Assessment of storm direct runoff and peak flow rates using improved SCS-CN models for selected forested watersheds in the Southeastern United States', *Journal of Hydrology: Regional Studies*, 27, p. 100645. doi: https://doi.org/10.1016/j.ejrh.2019.100645.Ye, F. *et al.* (2020) 'Simulating

storm surge and compound flooding events with a creek-to-ocean model: Importance of baroclinic effects', *Ocean Modelling*, 145, p. 101526. doi: https://doi.org/10.1016/j.ocemod.2019.101526.Zhang, W. *et al.* (2018) 'Urbanization exacerbated the rainfall and flooding caused by hurricane Harvey in Houston', *Nature*, 563(7731), pp. 384–388. doi: 10.1038/s41586-018-0676-z.USDA 2022. US Department of Agriculture. Geospatial data access. Available at. https://datagateway.nrcs.usda.gov/. Accessed on 01/1/2021

Weather Underground 2022.Weather Underground provides local & long-range weather forecasts, weather reports, maps & tropical weather conditions for locations worldwide. Available at: https://www.wunderground.com/. Accessed on 05/01/2021

NOAA 2022. NOAA Tides and Current. Available at: https://tidesandcurrents.noaa.gov/. Accessed on 01/05/2022

USGS 2022a. US Geological Survey. South Carolina Data Archive. Available at. https://water.usgs.gov/floods/events/2015/Joaquin/data_ofr20161019/. Accessed on 01/01/2022

USGS 2022b. 3D Elevation Program. Available at: https://www.usgs.gov/3d-elevation-program. Accessed on 01/01/2022